Measurement 146 (2019) 241–253

Contents lists available at ScienceDirect

Measurement

journal homepage: www.elsevier.com/locate/measurement

Development of an Arduino101-LoRa based wind speed estimator

Mehrdad Babazadeh, Kianoosh Karimi

Faculty of Engineering, University of Zanjan, University Blvd., Zanjan, Iran

A R T I C L E I N F O

Article history:
Received 4 January 2019
Received in revised form 21 May 2019
Accepted 10 June 2019
Available online 20 June 2019

Keywords:
Wind speed estimation
Anemometer
Wireless sensor network
LoRa
Arduino101

A B S T R A C T

An inventory application of a LoRa-based wireless sensor network on the wind turbines is described to replace anemometers with the low-cost and precise networked wind speed estimators. It operates without mechanical issues associated with the cup anemometers and provides better data even in the presence of turbulence, tower shadow, and nacelle body. Each node in this scheme compresses it's local real wind speed and electrical measurements and transmits corresponding packets to a center. Due to the limited memory and computational power available on the sensor side, the modeling task carries out primarily by the central node to eliminate the need for the anemometer. The nodes use the resultant linear multivariable model to estimate the local wind speed instead of using the anemometer. The methodology can be applied to the AC or DC turbines with an excellent performance where the LoRa technology minimizes power consumption while maximizing the license-free communication range.

1. Introduction

The demands for the precise wind speed measurements is growing in different areas such as the meteorology, aviation, railway, military, roadside weather stations, and wind industry in particular. Authors in [1] introduce the wind speed measuring instrument and its principle and structure characteristics for wind power generation systems. Then, they analyze the advantages and disadvantages of various wind speed measurement methods.

There are a few known wind speed measuring methods as follows:

- Mechanical methods by using anemometers as introduced in [2–4]. The mechanical cup anemometers are massively used with the Wind Turbine Generators (WTGs), on top of the WTGs, measuring the wind speed. The cup anemometers are prone to mechanical wear and corrosion issues [5] and may need maintenance. According to [6], the cup anemometers are with their generic limitations, the principal ones being related to:
  – Non-ideal sensitivity to angle of attacks outwith the horizontal plane
  – dynamic response
  – non-linearity of calibration and variation in calibration caused by mechanical friction or due to the shape of the cups
  – In some cases changes in calibration sensitivity with horizontal wind direction

  The first-class products are more corrosion resistant today. As proof for this, in [7], they evaluate the effect of wind tower shading, aging of wind anemometers and variation of mean turbulence intensities at the wind measurement site during 55 months. Their study shows that the performance of the sensors didn't deteriorate much with time but slightly higher values of tower distortion factor obtained with the passage of time.
- Thermal anemometers as mentioned in [8–12] are accurate measuring devices though they have a limited range of operation.
- Remote sensing- In a long time recording scenario, a cup anemometer needs met masts for mounting where the associated costs of the purchase, erection, and instrumentation increases with height. The evolution of high power WTGs has resulted in increased hub heights, thus making remote sensing an important issue for wind energy applications. Remote sensing can determine wind speed and direction at different heights using a ground-based instrument operating via the transmission and detection of light (LIDAR) or sound (SODAR) as discussed in [13]. More details about remote sensing can be found in [14–19].

  Authors in [20,21] evaluate the dynamic action on the bridge induced by the turbulence wind. They include 3D ultrasonic anemometers in the structural health monitoring system to collect wind data. Further, field data is gathered and comparative study is conducted to investigate the boundary layer wind characteristics and wind effects on the super-tall buildings in [22]. Authors of another article, [23] use Floating Lidar Systems

E-mail address: mebab@znu.ac.ir (M. Babazadeh)

https://doi.org/10.1016/j.measurement.2019.06.020
0263-2241/

Nomenclature

ω_{est}	estimated wind speed
ω_{real}	real wind speed
τ_e	electrical torque caused by turbine load
τ_w	mechanical torque exerted by the wind to the turbine
τ_{est}	estimated input torque to WTG
e_w	wind speed error
I_g	generator output current
I_{Load}	main load current
LS	least square method
SN	sensor node
SS model	state space model
V_a	input voltage of buck/boost converter
V_{ref}	reference voltage used in estimator
WSN	wireless sensor network
WTG	wind turbine generator

(FLS) to replace an offshore met mast, being significantly cheaper and saving an essential part of project upfront investment costs. They need to overcome the movement of the sea imparting motion on the Lidar, and maintaining wind speed and direction accuracy.
The remote sensing methods are the most accurate but also the most expensive which are not usual to be employed for the real-time wind speed measurement in WTGs as is the aim of the present research.

- Other techniques- In [24], they report a methodology, suitable for IC integration with MEMS technology, that offers reliable performance on the wind speed measurement in the range 0–20 m/s with a precision of about 2.5%.
Researchers in [25] apply direct and inverse modeling of the wind turbine and in [26], they use online training neural network-based algorithm for wind speed estimation. Another article, [27] introduces an extreme learning machine approach for sensor-less wind speed estimation. The inputs for estimating the wind speed are wind turbine power coefficient, blade pitch angle, and rotational speed. They claim that they get better results than other methods like neural networks etc. [28] focuses on the Kalman filter used for wind speed estimation and [29] compares a nonlinear *Takagi Sugeno* observer for wind speed estimation with enhanced Kalman Filter techniques.

According to the above-mentioned methodologies, two types of wind measurements may be conducted before or after the creation of a wind power site or even a WTG:

- A long term wind speed recording, usually more than a year, for the potential wind energy evaluation of the site. This measurement is not focused on this research.
- A real-time wind speed measurement as the feedback for the WTG's local controller and/or for the power plant controller in which the present research focuses on this type of measurement.

The nacelle anemometer is supposed to measure the free real-time wind speed. However, the flow around the nacelle is turbulent due to numerous sources of disturbances such as blades rotation, rotor geometry, tower shadow and the nacelle body as mentioned in [30–33]. This is why the present applied research aims to replace the mechanical cup anemometers with an accurate, flexible multi-variable model.

In the proposed wireless network-based system, a state space model (*SS model*) is primarily made by a central node having the measured wind speed and other electrical variables. In the next stage, each Sensor Node (SN) estimates the wind speed (ω_{est}) having the model and real-time electrical variables. The estimators, sensor nodes are implemented in a wireless platform to gain more flexibility for further developments. They can include extra functionality like wireless data acquisition and anomaly detection towards less supervision and more reliability. Although the cost of the wired anemometers is comparable to other equipment just in the low-power WTGs, having a low-noise reliable wind speed estimation will be an added value regardless of WTG's power level which is one of the main contributions of this research. Implementing on a single-core processor, it is for the first time in this paper to represent both practical and simulation results of an inventory WSN based wind estimation by employing the long range, LoRa technology.

For the sake of simplicity of discussions in the proposed simulations, a DC power wind turbine is modeled although the methodology can also be extended to AC power WTGs which are more usual in the higher power. The extension is straightforward since a black-box *SS model* is made from the known electrical inputs to the wind speed. The measured signals of the generator are available both in DC and AC systems and the rest of the modeling procedure is quite similar for both systems. Installation of the developed system on a real WTG is in a future plan.

The present article is summarized in a few sections as follows: Section 2 briefly refers to the system overview. The next Section 3, briefly addresses different units in the implemented Arduino101-LoRa based estimator and their functionality. A black-box linear state-space model is made in Section 4 where the center-side model and the sensor side utilization is supported by simulations.

2. System overview

The revolving-cup anemometers are widely used for the wind-speed measurements in a 3-wire configuration as seen in Fig. 1. They need electric power and enough wind speed to revolve. Since the output signal frequency is proportional to the real wind speed, they provide a logical output which is simply used to calculate the wind speed.

The useful wind speeds range from 4 m/s to 16 m/s for most WTGs. Within this range, anemometer accuracy and measurement repeatability are of utmost importance. Having lower measurement error is important because it is amplified to the 3rd power while it is translated to electrical power production.

According to the proposed methodology, as shown in Fig. 2, the anemometer is supposed to be replaced with a WSN-based estimator to offer an economical, tolerant, and flexible solution. SNs locate on top of the WTGs possibly far away from each other and/or from a center. They compress various measured data and store them in their own SD memory card. Then, transmit the compressed data to the remote center in a way the transmission occurs with the minimum payload in a timely manner. The center then decompresses the received compressed data, uses the already made model for further supervisory and/or control purposes. There are three types of data packets for communication as follows:

- $D_x(i,k)$: xth compressed data packet, transmitted by SN_i to the center (SN_k).

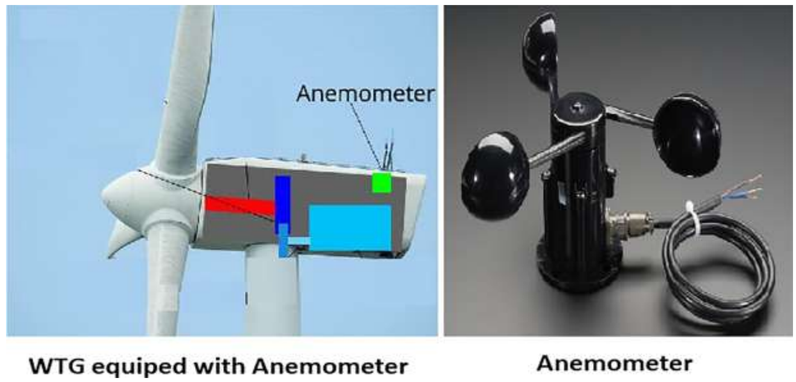

Fig. 1. WTG with anemometer installed (left) and Revolving-cup anemometer (right).

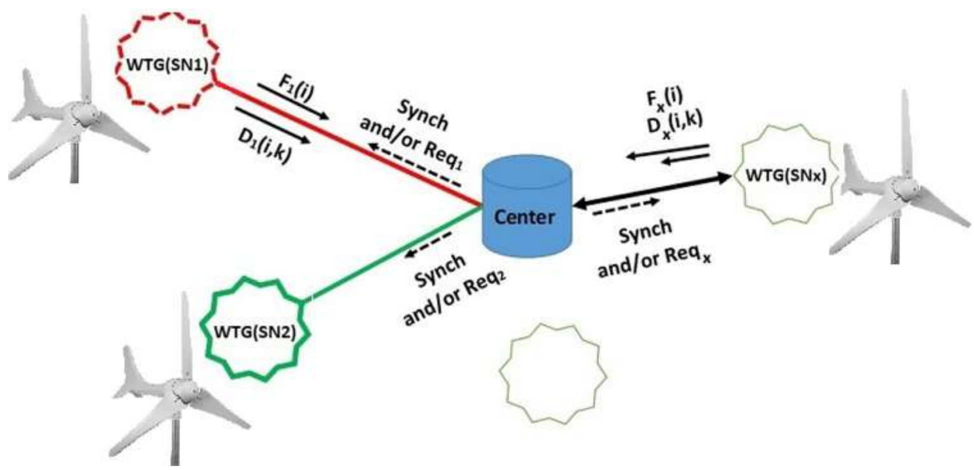

Fig. 2. SNs located far away from center on WTGs.

- $F_x(i)$: the xth management data packet, generated by SN_i for notifications.
- Synchronization command, data request, settings etc.

Depending on the turbine type and the voltage, a buck/boost converter might be needed to step delivered voltage from WTG up or down in order to charge the batteries as illustrated in Fig. 3. This model is used in the simulations throughout the paper.

3. Implementation of Arduino101-LoRa based SN

As shown in Fig. 4, an SN includes the following units to perform the required functionality:

- Main processor, Arduino 101.
- SD card shield: to record compressed data. The volume can be whatever more than 1 GB to keep a few months of data.

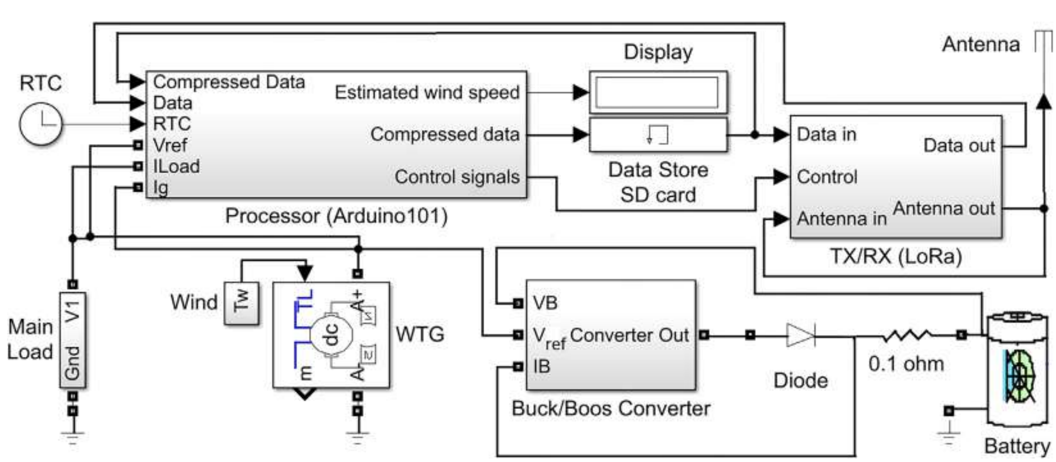

Fig. 3. System overview including SN, Buck/Boost converter, WTG, and battery pack.

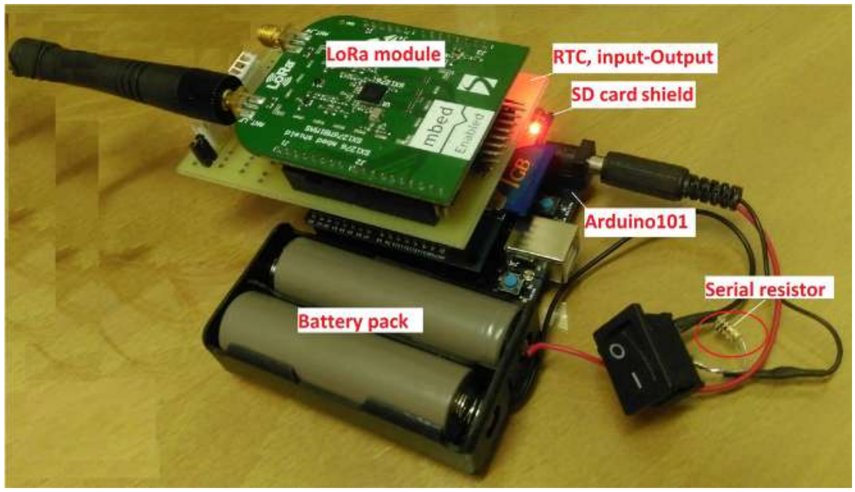

Fig. 4. Developed Arduino101-LoRa module as estimator SN.

- Real-time Clock (RTC) and expansion board: to keep real-time clock for SNs and terminals for input–output signals.
- A low power, wide range communication technology, LoRa shield (SX1276MB1MAS).
- Battery pack to supply SN while needed.

3.1. Arduino101 as the main processor

In the center-side, Arduino101 is used to implement the data management, the wind speed estimator, and also the system identification algorithm. It is noteworthy that the identification algorithm is only used in the first stage where a model is made based on the real wind speed measurements and the other data. In the sensor-side, the compression algorithm [34], data acquisition, and other control tasks are implemented.

3.2. SD memory card

Fast incoming measured data cannot be transmitted out immediately by the slow LoRa communication. They have to be compressed in size first, stored, and then be transmitted if requested by the center. To make this possible, an SD memory card is needed to store compressed data. In addition, a long history of data can be recorded for future needs. Then, there will be two options for communication of each SN with:

- A gateway (center): In case there are numbers of WTGs in the network, the compressed data might not be transmitted simultaneously unless there are a powerful gateway and appropriate regulations in place. A more expensive but faster option.
- Another node as the center (node to node): The SNs need to check the channel first and transmit data in case the channel is free. A cheaper but slower option.

3.3. Real time clock

The SNs have variable transmitting delay times since they work independently and that they have to verify the free channels before they transmit. Each compressed data packet must include a timestamp in order for the center to know which SN and when measured the data. The real-time clock (RTC) keeps clock time for the SNs and can be synchronized by the center (implemented in this research). The clock time of each SN can also be provided independently by a GPS module which is the more expensive solution.

3.4. LoRa module

To make a star topology of WTGs located in a wide area, the LoRa technology used where the hardware had already been developed and reported in [34,35] and the software customized accordingly for the present application.

3.5. Battery pack

The SN was designed to be supplied either by two series lithium-ion batteries (while WTG is not operating) or by a buck/boost converter for operational WTGs. The batteries are charged via the buck/boost converter to ensure enough power exists to stay operational for the processing and communication tasks. Fig. 4 showed two 3.3 V, 2200 VAh, Li-Ion batteries in series connection to provide enough voltage in the range 6–10 V to supply Arduino101 and the peripherals.

4. Center-made model of the system

Despite an off-load generator, the terminal voltage of an on-load WTG of either type (fixed or variable rotor speed) can change due to the variations in the local controller's regulatory operation, the load demand, and the weather characteristics (wind speed, humidity, weather density, pressure, etc.). As shown in Fig. 5, the input from an off-load anemometer provides real rotor angular speed ω_{real} to obtain the wind speed error ($e_w = \omega_{real} - \omega_{est}$) only during the parameter estimation phase. According to Fig. 6, a variable mechanical input torque (τ_w) is used as the representative of the wind speed fed to the generator shaft to highlight the relationship between the rotor speed and the wind speed due to the load variation. In this relation, τ_e is the torque created by the load current in the reverse direction. It is noted that the direction of a WTG is always controlled by the Yaw system. Therefore, the wind direction is inherently integrated with wind speed estimation. The "Load" block in this scheme consists of a buck/boost branch which is connected to the battery and the processor, in parallel with the main load. In the end, the load effect on the rotor speed is seen in the targeted black-box model of the system. The difference between τ_w and τ_e is the resultant torque of the rotor which has linear dynamic relation with ω_{real}. This ω_{real} in a DC or AC generator is approximately proportional to the generated back emf voltage (V_{emf}). Instead, the terminal voltage (V_a) in Fig. 6 is affected by both load current and wind characteristics. Obviously, V_{emf} and V_a dif-

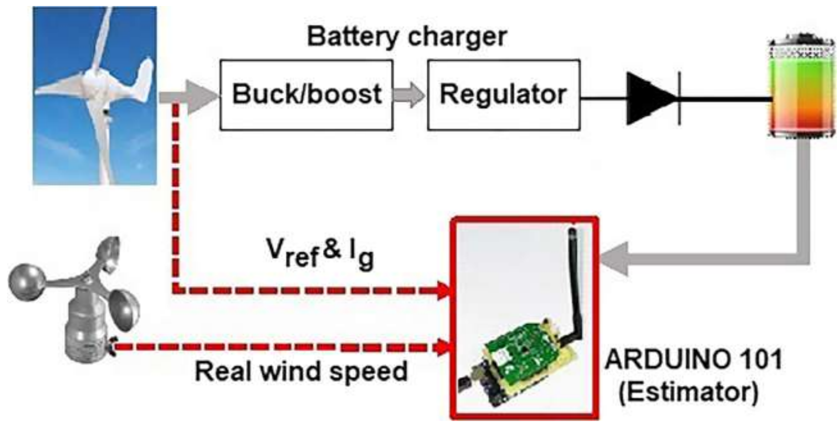

Fig. 5. Anemo-Modeling system used in the modeling stage.

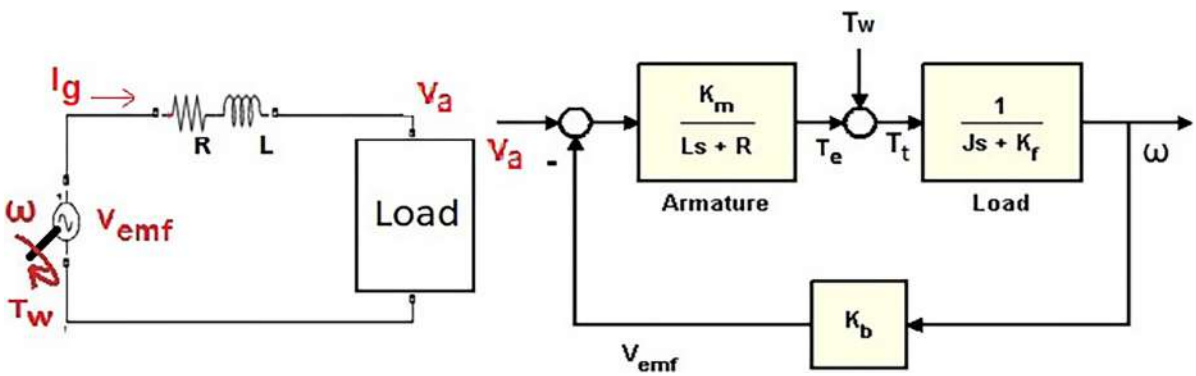

Fig. 6. Interactions between electrical and mechanical parameters of a typical DC generator.

fers because of the total voltage drop on the generator's inductance and resistance. The proposed system including the WTG, buck/boost converter, load, and the battery will be represented by a black box *SS model* in the next subsections.

4.1. Input-output selection

Configuring the system identification method, allocation of the independent electrical inputs and the available output, ω_{real} (or τ_w in simulation) was taken into account. Then, a random noise represented the unknown variables. The measured inputs and output signals sampled at the maximal sampling rate achievable for the SN that could be handled based on the developed hardware (1 kHz). In this scheme, V_{emf} can be calculated either based on the measured angular speed or by measuring V_a and the generator output current (I_g). Therefore, V_{emf} is not an independent variable and is not considered as the input in the proposed state space model. The modeling of the excitation signals are discussed in the next sections and the system identification is carried out afterward.

4.2. Simulated wind and real wind model

Fig. 7 represents a model where a series of simulated wind speed data generates τ_w for the WTG. Then, the resultant correlation between the signals shown in Fig. 8, the generator reference voltage (V_{ref}), and current (I_g) are chosen as inputs of the model and τ_w, proportional to ω_{real}, is considered as the output. In addition, another series of the real wind speed data which has been measured by an anemometer [36] generates a realistic profile of τ_w which is used later in an extra model validation (see Section 4.5).

As already represented in Fig. 2, the load for WTG is a combination of the main load (conventional load in the range of W, kW or MW) and a partial load (due to the interaction between the battery, Arduino101, and peripheral which is less than 1W). Therefore, the source for the wind speed estimation cannot be made only based on the rotor speed due to the load effect.

4.3. Load model

According to [34,35], for the simulation purpose, the consumed power by Arduino101-based SN is extracted from a laboratory test illustrated in Fig. 9. In addition, the main load model as a combination of a resistive load and an independent current source is represented in Fig. 10 where the size of the partial load of SN can be negligible in the large power WTGs. As seen in Fig. 11, a prepared module, MT3608 [37] is used as the DC-DC converter due to the low power dissipation, wide input voltage range (2 V–24 V) and appropriate maximum output current (2A) and voltage (up to 28 V). To provide appropriate charge current for the battery pack, the output voltage is set to supply lower charge current than 600 mA during the worst case situations where the lowest battery charge exists.

4.3.1. System model

The *SS model* is formulated in the following where $u(t), x(t), k$, and D are vectors of size (2×1), (3×1), (3×3), and (1×3). Input vector, $u(t)$ includes I_g and V_{ref}. The next two parameters, k and D are assumed zero in this simulation just for a simple presentation.

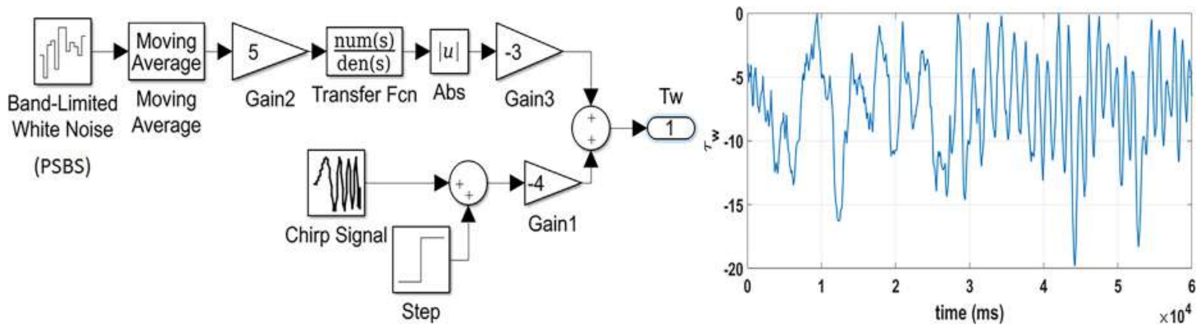

Fig. 7. Model (left) and diagram (right) of the produced τ_w as the representative of the wind speed.

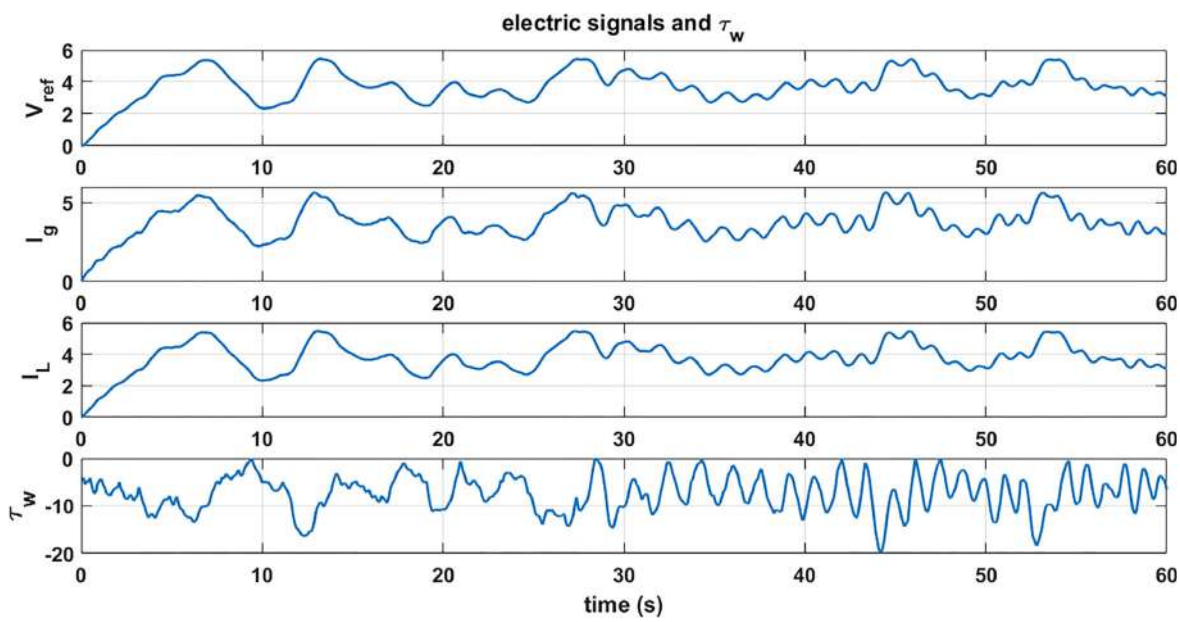

Fig. 8. Affected electrical signals when the system is excited by a modeled variable τ_w.

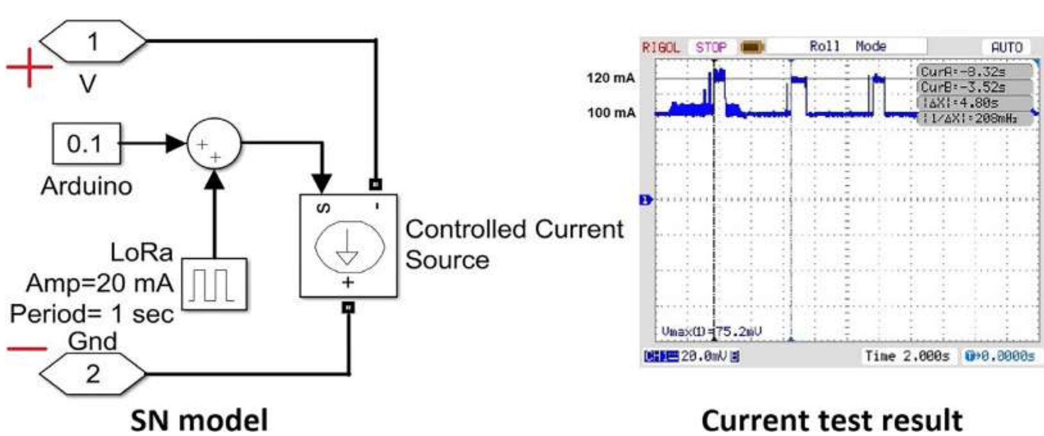

Fig. 9. Partial load model (left) and consumed current by SN (right).

$$
\begin{aligned}
\dot{x}(t) &= A \times x(t) + B \times u(t) + k \times e(t) \\
y(t) &= C \times x(t) + D \times u(t) + e(t)
\end{aligned}
\tag{1}
$$

According to the methodologies proposed in [38] modeling task is conducted in this research. The provided data is generated by the wind and load models which were given in Sections 4.2 and 4.3, the proposed *SS model* is verified after parameter estimation is applied by the system identification toolbox (Ident) as follows:

$$
A = \begin{bmatrix} -0.2118 & 0.1287 & 0.0301 \\ 0.1053 & 0.329 & -0.4884 \\ 0.7268 & -0.1401 & -0.4322 \end{bmatrix}; \; B = \begin{bmatrix} -5779 & -927.3 \\ 3.465e4 & 5533 \\ 7.148e4 & 1.137e4 \end{bmatrix}
\tag{2}
$$
$$
C = [1.413 \;\; 0.07224 \;\; 0.02787]; \; D = [0 \;\; 0]
$$

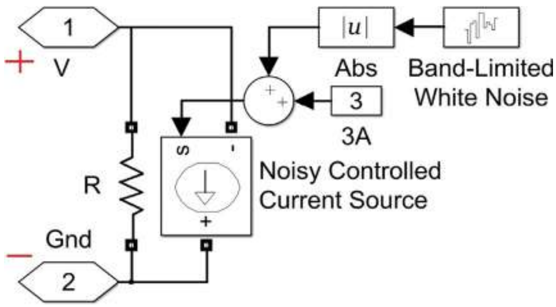

Fig. 10. Main load model as a combination of a resistor and a dependent current source.

It is noteworthy to mention that the '*Best Fit*' model is obtained with a higher order than eight as depicted in Fig. 12. However, according to '*AKAIKE*' criterion, the third order model is selected here regardless of its inherent relative inaccuracy to respect both the simplicity and accuracy.

4.4. Final model validation based on simulated wind data

As mentioned, to make a generator model with variable rotor speed due to the load change, a variable τ_w is applied instead of ω_{real}. Therefore, τ_{est} is the output which can be simply converted to the ω_{est}. In practice, where ω_{real} is available from the anemometer, it will be used instead of the τ_w. The SN supposed to provide an accurate ω_{est} in order to eliminate the anemometer. This is tested by simulating the system represented in Fig. 13 in different operating circumstances through the next subsections.

4.4.1. Obtained model validation while both wind speed and load change

The system is excited with rich excitation signals from both excitation points (wind and load) in order to attain the best possible state space model. By using the MATLAB Ident, an *SS model* is properly identified and the comparative diagram of the estimated and original data is shown in Fig. 14 with 96.63 % fit value. In the next section, it will be seen that the obtained linear model is a suitable representative of the anemometer. This can be used in the simulation with two inputs (V_{ref} and I_g) with the results represented in Fig. 15. The model output is not as accurate as the result obtained by Ident (compare Figs. 14 and 15). Because, the precise parameter values are internally used by Ident where Ident reports approximated values for model parameters that make a round-off error when they are applied to an *SS model* in the simulation phase. Therefore, it could be more accurate if the original numbers were available. The identified system is successfully validated with different random excitation signals for both τ_w and I_{load} in Ident and Simulink. The results are shown in Figs. 16 and 17.

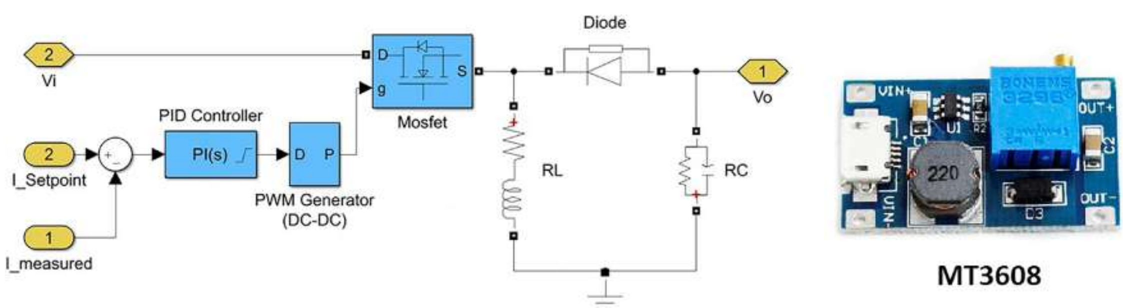

Fig. 11. Buck/boost converter, simulated scheme (left) and utilized MT3608 (right).

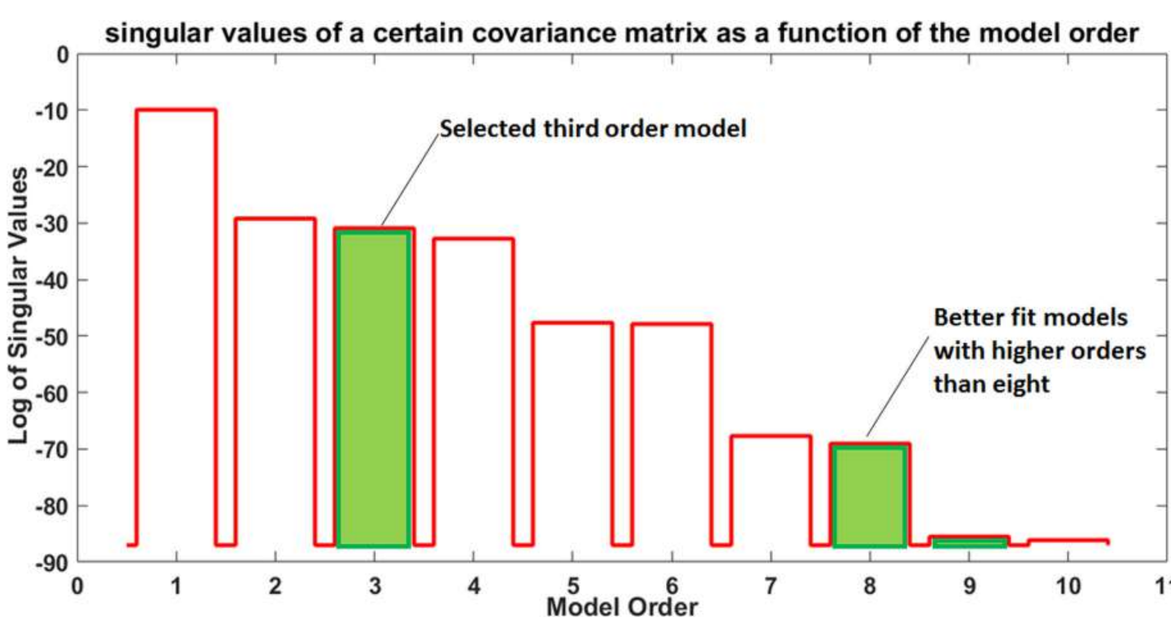

Fig. 12. Singular values of a certain covariance matrix constructed from the observed data as a function of the model order.

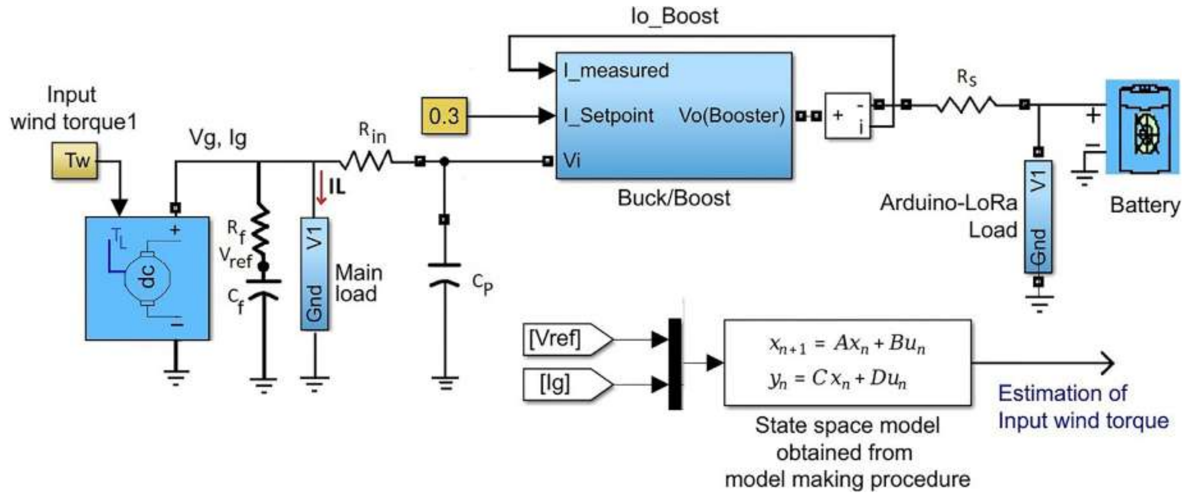

Fig. 13. Full model, including the obtained *SS model* for simulation.

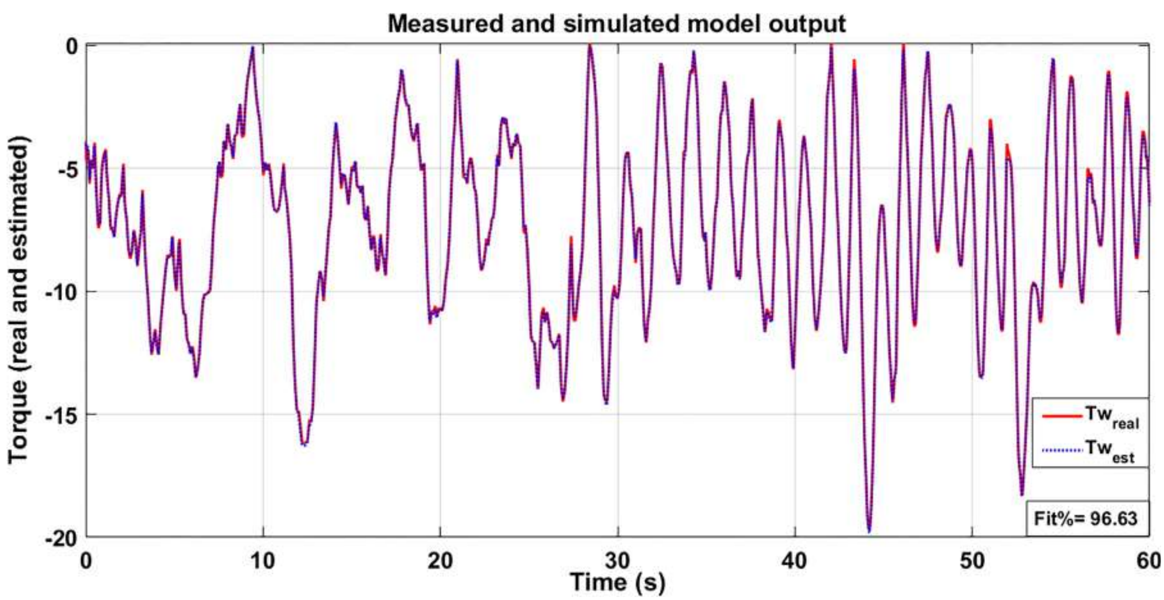

Fig. 14. Comparison of τ_w and provided τ_{est} by the *SS model* in model making stage in Ident.

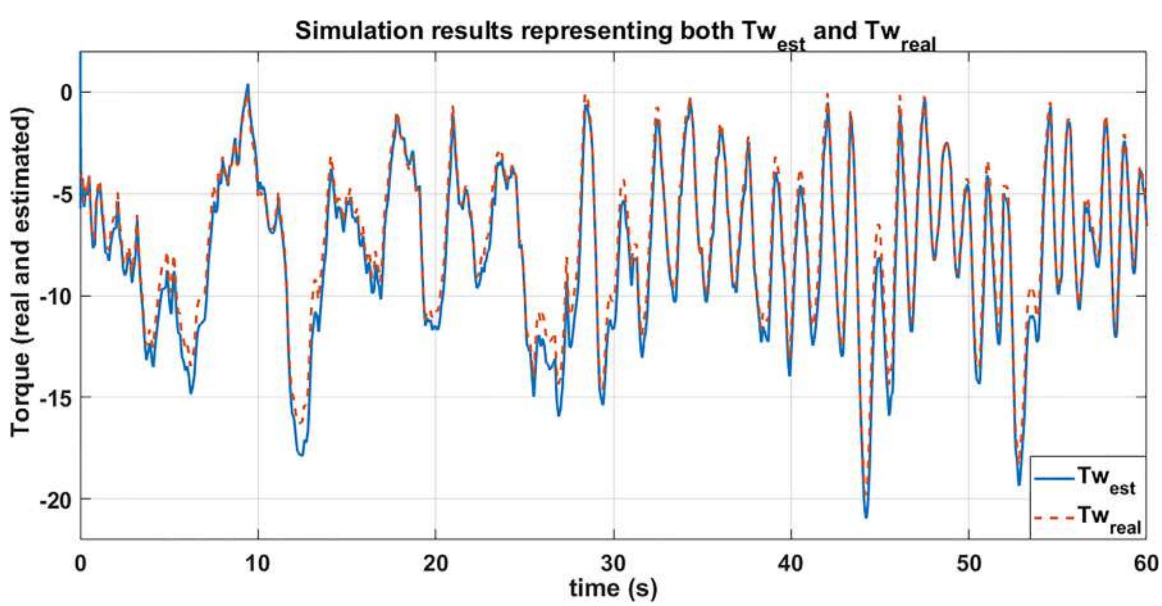

Fig. 15. Comparison of τ_w and provided τ_{est} by the *SS model* in simulation stage.

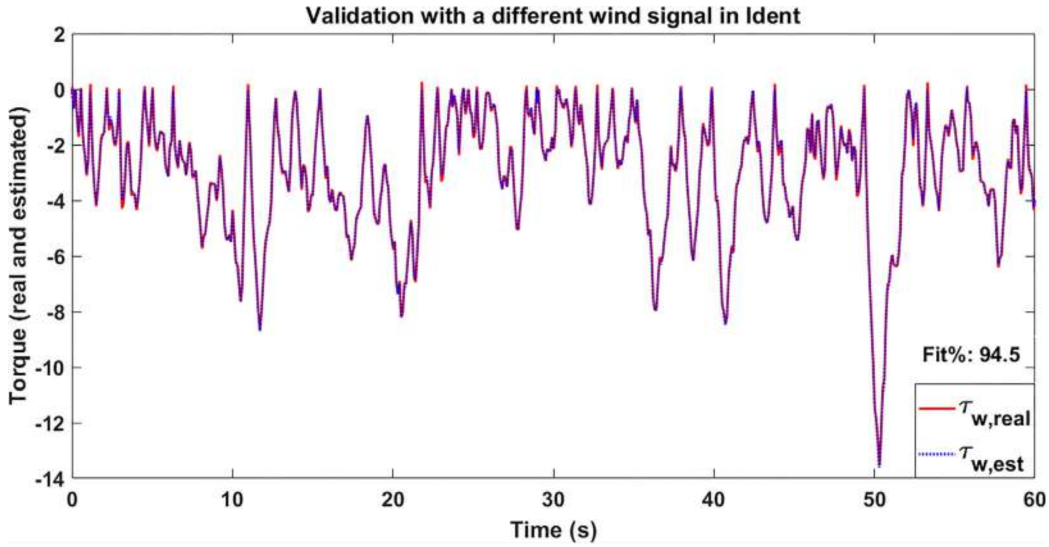

Fig. 16. Validation results by comparing τ_w as a different random wind and provided τ_{est} in Ident.

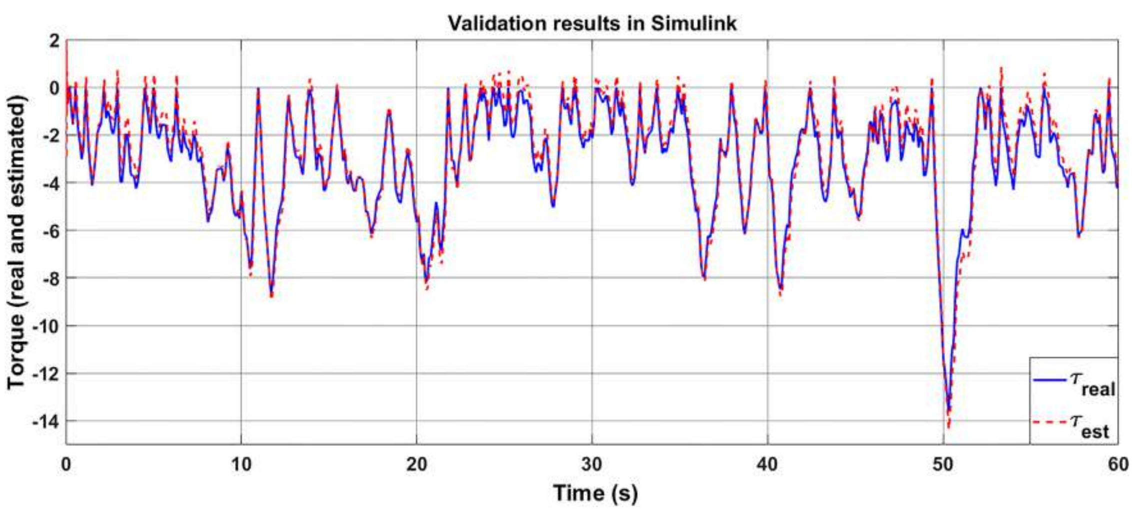

Fig. 17. Validation results with different random excitation signals by the constructed state space model in Simulink.

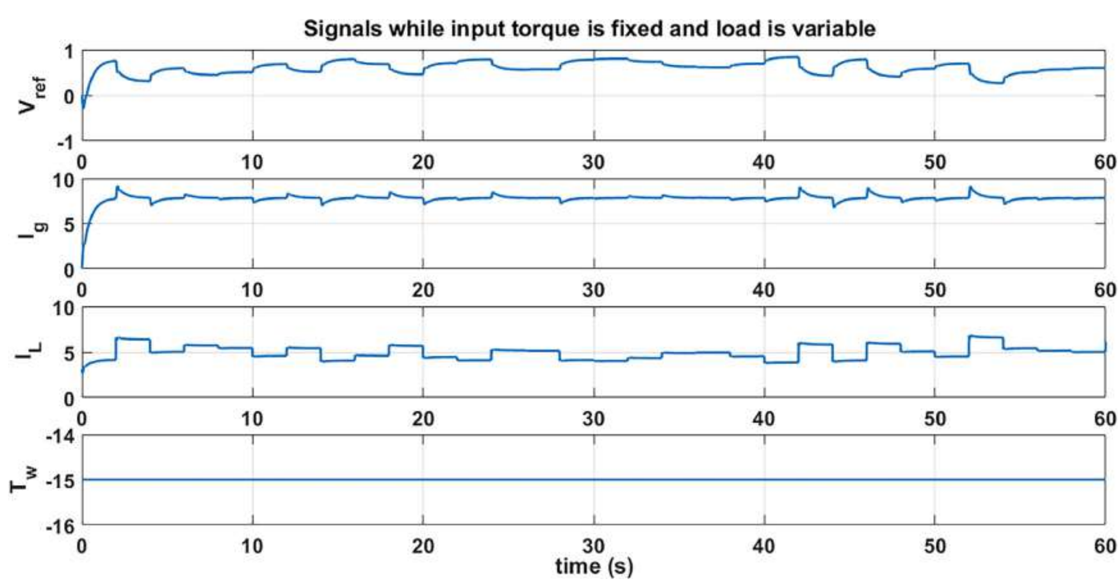

Fig. 18. Affected electrical signals while τ_w keeps fixed.

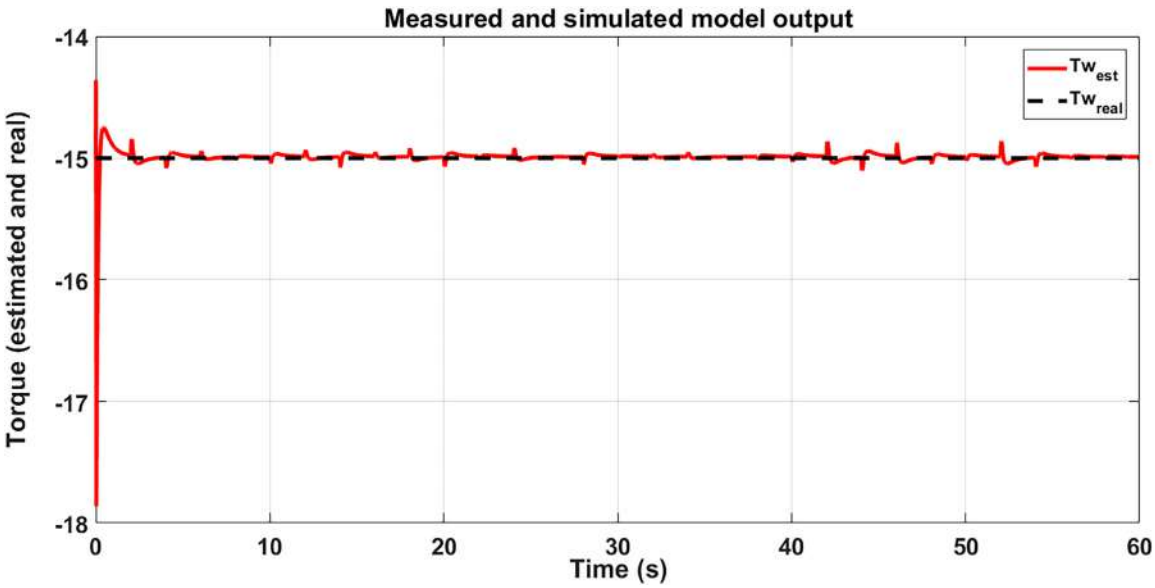

Fig. 19. Detecting a constant torque by electric signals excited by a random load.

4.4.2. Constant wind speed (or torque in simulation) with variable load

The SN in this validation test estimates τ_w by the given electric input signals while the load varies randomly as denoted in Fig. 18. The next Fig. 19 represents an excellent fit between τ_w and τ_{est} that verifies the obtained model's relative accuracy.

4.4.3. Constant load with variable wind speed (or torque in simulation)

The SN in this stage estimates the variable wind torque by the given electric input signals while the load is fixed. Fig. 20 represents important signals while I_L, the main load current is constant. Fig. 21 denotes excellent fit between τ_w and τ_{est} that verifies the obtained model accuracy.

4.5. Model validation by using real measured wind speed data

Additionally, the acquired model is validated by real wind speed data published in [36]. The diagram of the wind speed is represented in Fig. 22. The mechanical torque caused by the wind is applied to the model in Simulink which is always negative in generator mode of electric machines. The validation diagram, represented in Fig. 23 indicates a very good fit between the estimation (generated by the developed model) and the real measurement data. The diagram of the estimation error is as the following Fig. 24.

5. Conclusions

An invention to replace the wind turbine's anemometer with a wind speed estimator in a wireless sensor network platform described in the present work. The method could offer high accuracy and low cost which can be applied in different types of wind turbines, AC or DC. The turbine supplies power to the conventional load and to the proposed Arduino101-LoRa based sensor node. The LoRa module is used to transmit the compressed data in a long range with minimal power consumption. Applicable even for the

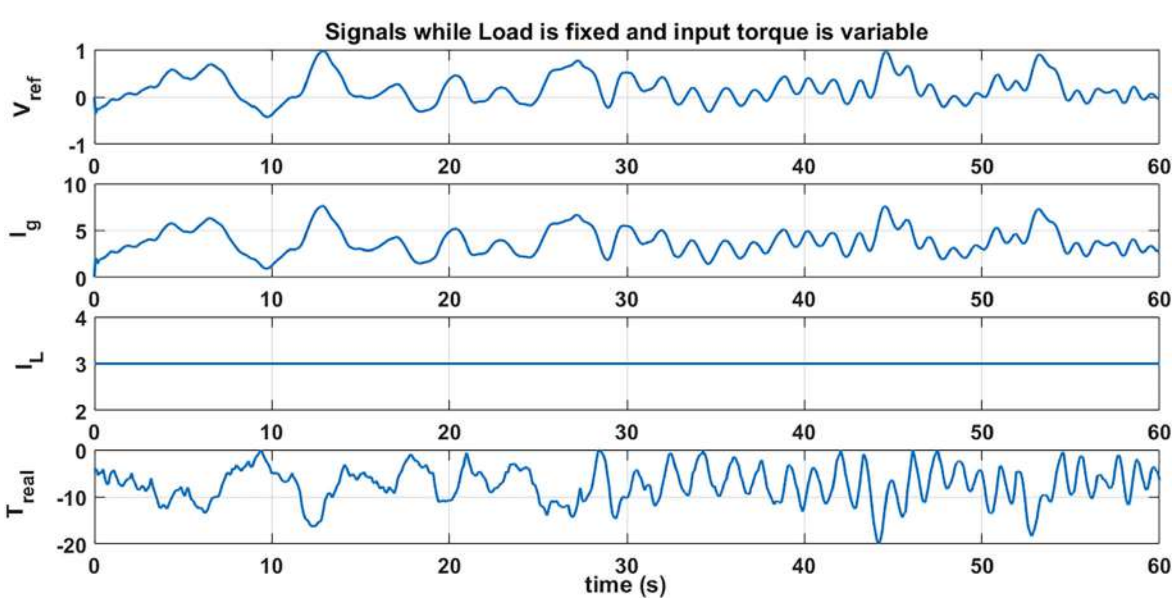

Fig. 20. Important signals while the main load keeps fixed.

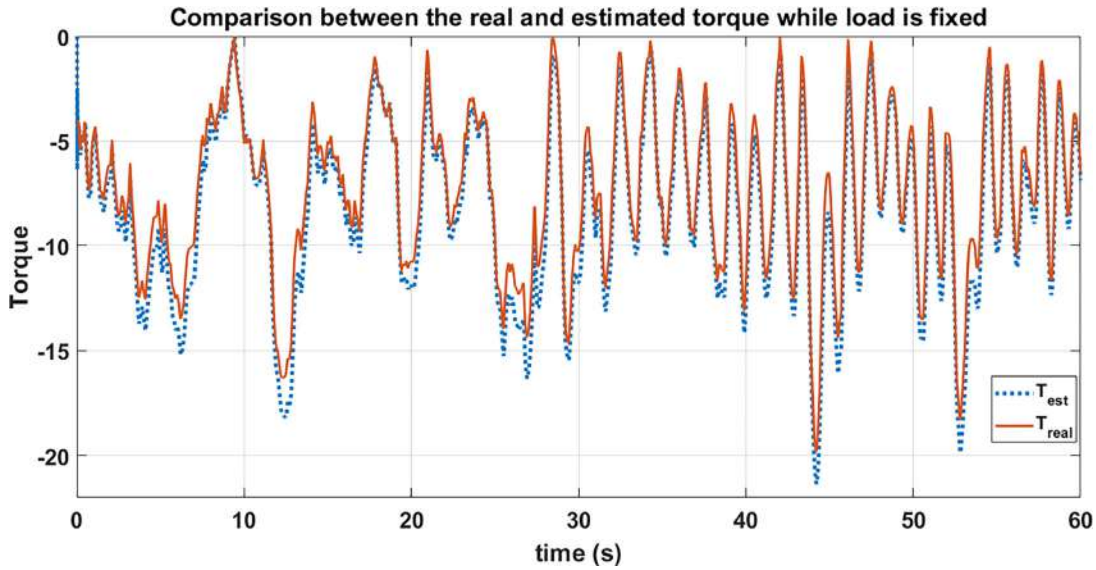

Fig. 21. Estimated torque obtained by the *SS model* vs. real torque (generated by simulated wind speed) while the load is fixed.

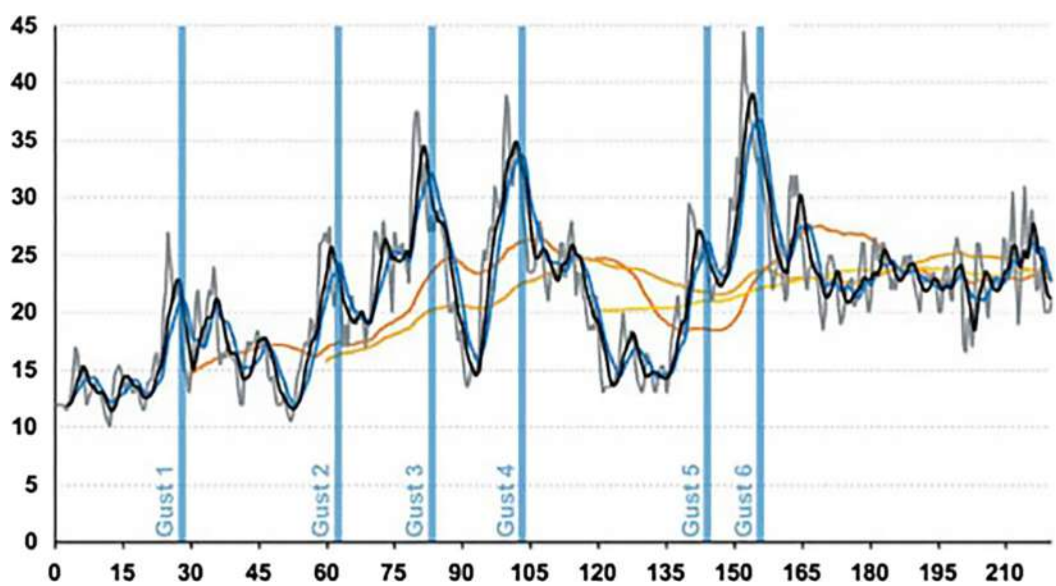

Fig. 22. Real wind speed waveform published in [36].

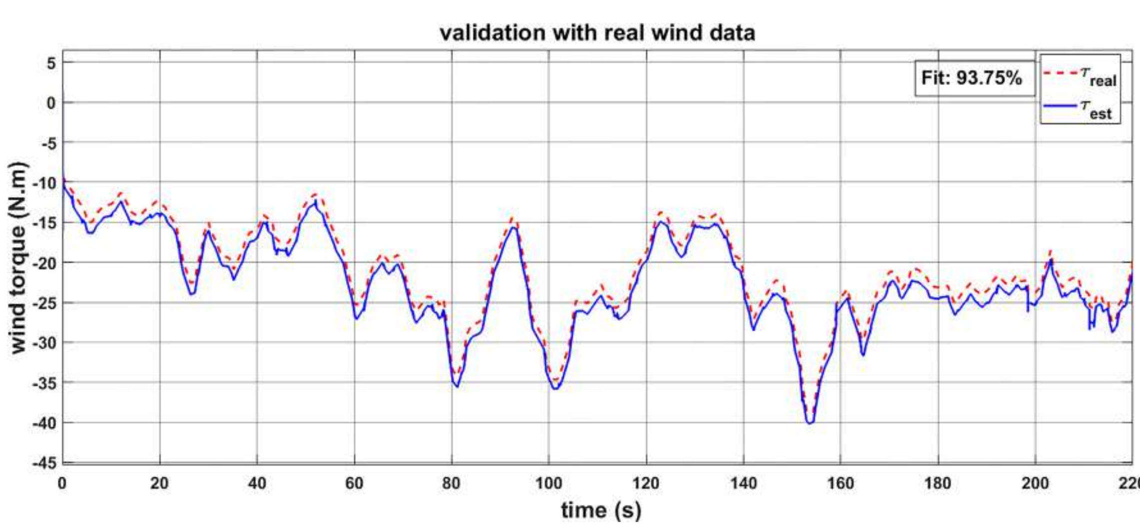

Fig. 23. Estimated vs. real measured wind speed (wind torque).

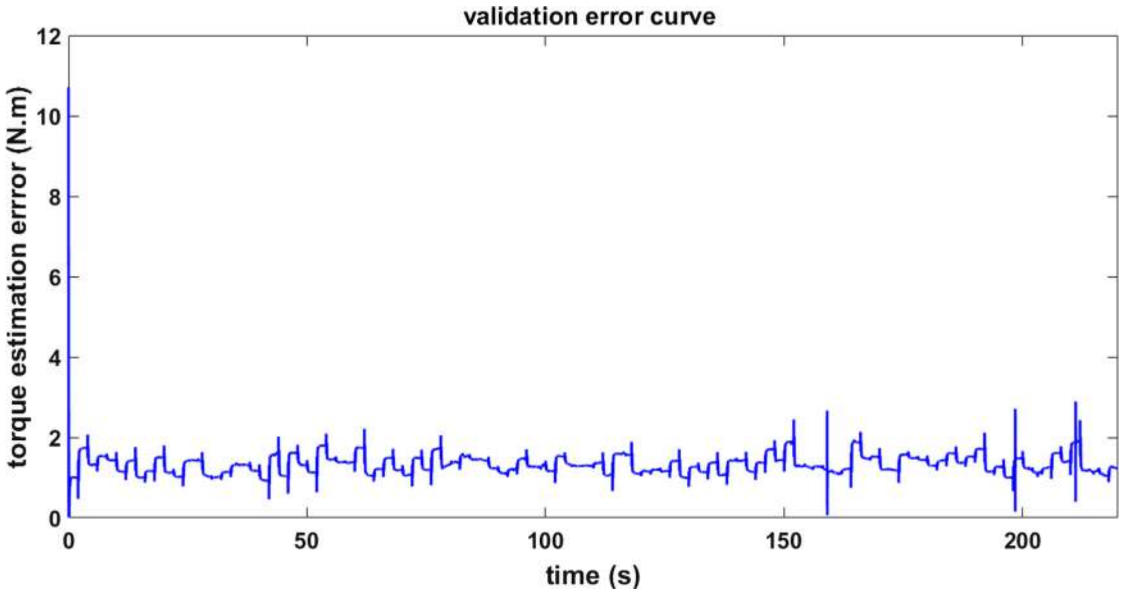

Fig. 24. The error curve in all seconds of the simulation with real wind data.

low power turbines, the implemented system in the sensor-side works operator-free and communicates compressed data with the minimum payload for possible control or supervisory actions in the center. In particular, the measured data including wind speed and some electrical variables are used in the center side to make a model for the source sensor nodes. The model parameters are transmitted to the node to be used for the real-time wind speed estimation.

Declaration of Competing Interest

None.

References

[1] L. Peng, L. Wenhong, Z. Shuai, Q. Tianshuang, Wind speed measurement technology in wind power generation system, Microcomput. Inf. 14 (2015) 3.
[2] Y.P. Solov'ev, A. Korovushkin, Y.N. Toloknov, Characteristics of a cup anemometer and a procedure of measuring the wind velocity, Phys. Oceanogr. (2004) 173–186.
[3] J. Wyngaard, Cup, propeller, vane, and sonic anemometers in turbulence research, Annu. Rev. Fluid Mech. 13 (1) (1981) 399–423.
[4] P. Hyson, Cup anemometer response to fluctuating wind speeds, J. Appl. Meteorol. 11 (5) (1972) 843–848.
[5] C. Azorin-Molina, J. Asin, T.R. McVicar, L. Minola, J.I. Lopez-Moreno, S.M. Vicente-Serrano, D. Chen, Evaluating anemometer drift: a statistical approach to correct biases in wind speed measurement, Atmos. Res. 203 (2018) 175–188.
[6] R.S. Hunter, B.M. Pedersen, T. Pedersen, H. Klug, N. van der Borg, N. Kelley, J. Dahlberg, Recommended practices for wind turbine testing and evaluation. 11. wind speed measurement and use of cup anemometry. 1, IEA, 2003, pp. 1–60..
[7] M.A. Baseer, J.P. Meyer, S. Rehman, M.M. Alam, L.M. Al-Hadhrami, A. Lashin, Performance evaluation of cup-anemometers and wind speed characteristics analysis, Renew. Energy 86 (2016) 733–744.
[8] Y. Zhu, B. Chen, M. Qin, Q.-A. Huang, 2-d micromachined thermal wind sensors – a review, IEEE Internet Things J. 1 (3) (2014) 216–232.
[9] H.-B. Liu, N. Lin, S.-S. Pan, J. Miao, L.K. Norford, High sensitivity, miniature, full 2-d anemometer based on mems hot-film sensors, IEEE Sens. J. 13 (5) (2013) 1914–1920.
[10] J. Chen, C. Liu, Development and characterization of surface micromachined, out-of-plane hot-wire anemometer, J. Microelectromech. Syst. 12 (6) (2003) 979–988.
[11] V. Stornelli, G. Ferri, A. Leoni, L. Pantoli, The assessment of wind conditions by means of hot wire sensors and a modifed wheatstone bridge architecture, Sens. Actuators A: Phys. 262 (2017) 130–139.
[12] R.M.P.D. Widyantara, H. Wind, direction sensor based on thermal anemometer for olfactory mobile robot, Indonesian J. Electr. Eng. Comput. Sci. 13 (2) (2019) 475–484.
[13] D. Dubov, B. Aprahamian, M. Aprahamian, Comparison of wind data measurment results of lidar device and calibrated cup anemometers mounted on a met mast), in: 2018 20th International Symposium on Electrical Apparatus and Technologies (SIELA), IEEE, 2018, pp. 1–4.
[14] G. Bucci, F. Ciancetta, E. Fiorucci, D. Gallo, C. Landi, M. Luiso, A low-cost ultrasonic wind speed and direction measurement system, in: Instrumentation and Measurement Technology Conference (I2MTC), 2013 IEEE International, IEEE, 2013, pp. 505–510.
[15] M.M. Costa, R.C.S. Freire, S.Y. Catunda, J.M.M. Villanueva, Wind speed measurement based on ultrasonic sensors using discrete fourier transform, in: Instrumentation and Measurement Technology Conference (I2MTC), 2013 IEEE International, IEEE, 2013, pp. 499–504.
[16] N.S.C. Ingaroca, J.M.M. Villanueva, R.C. Freire, S.Y. Catunda, Wind speed measurement method using ultrasonic sensors with stationary wavelet transform, in: Instrumentation and Measurement Technology Conference (I2MTC), 2012 IEEE International, IEEE, 2012, pp. 1759–1763.
[17] J.M.M. Villanueva, S.Y.C. Catunda, R. Tanscheit, Maximum-likelihood data fusion of phase-difference and threshold-detection techniques for wind-speed measurement, IEEE Trans. Instrum. Meas. 58 (7) (2009) 2189–2195.
[18] J.M. Sabatier, A.G. Petculescu, Doppler ultrasonic detection of targets buried in grass-covered soil, J. Acoust. Soc. Am. 115 (5) (2004) 2416.
[19] L. Yiding, W. Baoqiang, W. Yanjie, Time-difference ultrasonic wind detection methods based on cross-correlation theory, in: Electronic Measurement and Instruments, 2007. ICEMI'07. 8th International Conference on, IEEE, 2007, pp. 1-165–1-168.
[20] H. Wang, Z. Xu, T. Wu, J. Mao, Evolutionary power spectral density of recorded typhoons at sutong bridge using harmonic wavelets, J. Wind Eng. Ind. Aerodyn. 177 (2018) 197–212.
[21] H. Wang, A. Li, J. Niu, Z. Zong, J. Li, Long-term monitoring of wind characteristics at sutong bridge site, J. Wind Eng. Ind. Aerodyn. 115 (2013) 39–47.
[22] J. Fu, Q. Li, J. Wu, Y. Xiao, L. Song, Field measurements of boundary layer wind characteristics and wind-induced responses of super-tall buildings, J. Wind Eng. Ind. Aerodyn. 96 (8–9) (2008) 1332–1358.
[23] J. Gottschall, B. Gribben, D. Stein, I. Würth, Floating lidar as an advanced offshore wind speed measurement technique: current technology status and gap analysis in regard to full maturity, Wiley Interdiscip. Rev.: Energy Environ. 6 (5) (2017) e250.
[24] A. Leoni, V. Stornelli, L. Pantoli, A low-cost portable spherical directional anemometer for fixed points measurement, Sens. Actuators A: Phys. 280 (2018) 543–551.
[25] A. Accetta, M. Pucci, G. Cirrincione, M. Cirrincione, On-line wind speed estimation in im wind generation systems by using adaptive direct and inverse modelling of the wind turbine, in: Energy Conversion Congress and Exposition (ECCE), 2016 IEEE, IEEE, 2016, pp. 1–8.
[26] F. Jaramillo-Lopez, G. Kenne, F. Lamnabhi-Lagarrigue, A novel online training neural network-based algorithm for wind speed estimation and adaptive control of pmsg wind turbine system for maximum power extraction, Renew. Energy 86 (2016) 38–48.
[27] V. Nikolic, S. Motamedi, S. Shamshirband, D. Petkovic, S. Ch, M. Arif, Extreme learning machine approach for sensorless wind speed estimation, Mechatronics 34 (2016) 78–83.
[28] D. Song, J. Yang, M. Dong, Y.H. Joo, Kalman filter-based wind speed estimation for wind turbine control, Int. J. Control Autom. Syst. 15 (3) (2017) 1089–1096.

[29] E. Gauterin, P. Kammerer, M. Kühn, H. Schulte, Effective wind speed estimation: comparison between kalman filter and takagi–sugeno observer techniques, ISA Trans. 62 (2016) 60–72.
[30] A. Martínez, E. Vega, S. Pindado, E. Meseguer, L. García, Deviations of cup anemometer rotational speed measurements due to steady state harmonic accelerations of the rotor, Measurement 90 (2016) 483–490.
[31] K. Papadopoulos, N. Stefantos, U.S. Paulsen, E. Morfiadakis, Effects of turbulence and flow inclination on the performance of cup anemometers in the field, Bound.-Layer Meteorol. 101 (1) (2001) 77–107.
[32] Sanz-Andrés, S. Pindado, F. Sorribes-Palmer, Mathematical analysis of the effect of rotor geometry on cup anemometer response, Scientific World J. (2014).
[33] W.D. Lubitz, A. Michalak, Experimental and theoretical investigation of tower shadow impacts on anemometer measurements, J. Wind Eng. Ind. Aerodyn. 176 (2018) 112–119.
[34] M. Babazadeh, S. Kartakis, J.A. McCann, Highly-distributed sensor processing using iot for critical infrastructure monitoring, in: Proceedings of APSIPA Annual Summit and Conference 2017, APSIPA ASC 2017, 2017, pp. 1–10.
[35] M. Babazadeh, Edge analytics for anomaly detection in water networks by an arduino101-lora based wsn, ISA Trans. (2019).
[36] W. Read, The windstorms of 1995-2006: adjusting peak 5-second wind to better fit with past instant gust measures, 2008.URL:http://www.climate.washington.edu/stormking/StormRanksASOSadjusted.html..
[37] Aerosemi, High efficiency 1.2mhz 2a step up converter, mt3608, Aerosemi Technology Co., Ltd, 2018, pp. 1–7. URL:https://www.olimex.com/Products/Breadboarding/BB-PWR-3608/resources/MT3608.pdf.
[38] O. Nelles, Nonlinear System Identification: From Classical Approaches to Neural Networks and Fuzzy Models, Springer Science & Business Media, 2013.